Electronic Supplementary Material (ESI) for ChemComm.

Square Planar Cu(I) Stabilized by a Pyridinediimine Ligand

Pui Man Cheung,[a] Robert F. Berger,[a] Lev N. Zakharov[b] and John D. Gilbertson[a]

[a]Department of Chemistry, Western Washington University, Bellingham, Washington 98225, United States

[b]Department of Chemistry, University of Oregon, Eugene, Oregon 97403, United States

Table of Contents **Page**

Experimental

General considerations. Air sensitive materials were handled using standard Schlenk technique and stored under an MBraun glovebox (N_2) equipped with a cold well. All reagents were used as received unless otherwise noted. Aniline (≥99.8%), 2,6-diisopropylaniline (90%), 2,6-diacetylpyridine (99%), tetrakis(acetonitrile) copper(I) hexafluorophosphate ($[Cu(I)(CH_3CN)_4][PF_6]$) (97%) and tetrabutylammonium hexafluorophosphate ($TBAPF_6$) (≥99.0%) were purchased from Sigma-Aldrich Co. LLC. Anhydrous toluene and methanol were purchased from Fischer. Toluene, tetrahydrofuran and diethyl ether, and pentane were dried and deoxygenated with a PureSolv solvent purification system (CuO and alumina columns). Anhydrous acetonitrile (99.8%) and anhydrous dichloromethane (≥99.8%) were purchased from Sigma-Aldrich and used as received. Deuterated solvents, acetonitrile-d_3 (D, 99.8%) and tetrahydrofuran-d_8 (D, 99.95%), were purchased from Cambridge Isotope Laboratories, Inc. and stored under N_2. All solvents were degassed before use. Carbon monoxide (99.3%) was purchased from Airgas, Inc.

Infrared spectra were recorded on a Thermo Scientific Nicolet iS10 FT-IR spectrometer equipped with an ATR accessory. All NMR data were acquired on a Unity Inova FT-NMR 300 MHz spectrometer. ^1H spectra were recorded at either an operating frequency of 300 MHz or 500 MHz; $^{13}C\{^1H\}$ NMR spectra were recorded at an operating frequency of 75 MHz; $^{19}F\{^1H\}$ spectra were recorded at an operating frequency of 282 MHz; $^{31}P\{^1H\}$ spectra were recorded at an operating frequency of 121.5 MHz. Unless otherwise noted, all ^1H and $^{13}C\{^1H\}$ chemical shifts were reported with respect to an internal standard of $SiMe_4$ at 0 ppm; $^{19}F\{^{13}C\}$ and $^{31}P\{^1H\}$ chemical shifts were calibrated by external standards (trifluorotoluene in C_6D_6, -63.72 ppm and phosphoric acid in D_2O, 0 ppm, respectively). UV-Vis absorbance data were acquired using a Jasco UV-Vis/NIR spectrometer in a 1 cm quartz cuvette purchased from Starna Cells, Inc. Elemental analyses were performed by ALS (formerly Columbia Analytical Services) in Tuscon, AZ. Electronic paramagnetic resonance (EPR) spectra were recorded using a Bruker EMX spectrometer equipped with an ER041XG microwave bridge, an Oxford Instrument liquid-helium quartz cryostat, and a dual mode cavity (ER4116DM).

Ligand Synthesis. The literature procedure of synthesizing the pyridinediimine ligand, $^{i\text{Pr}}$PDI (2,6-(2,6-^{i}Pr$_2$C$_6$H$_3$N=CMe)$_2$C$_5$H$_3$N),[1] was modified to obtain a higher yield. 2,6-diacetylpyridine (1.90 g, 0.0116 mol) and excess 2,6-diisopropylaniline (4.0 g, 0.023 mol) was dissolved in c.a. 100 mL toluene with a catalytic amount of p-toluenesulfonic acid (22 mg, 0.12 mmol). The mixture was refluxed overnight. A yellow powder was obtained upon the complete removal of solvent with a rotary evaporator. Pure $^{i\text{Pr}}$PDI was obtained in 94% yield (5.26 g, 0.0109 mol) after washing with a small amount of reagent grade acetone.

The ^{H}PDI ligand (2,6-(C_6H_5N=CMe)$_2C_5H_3N$) was synthesized by the procedure described in the literature.[2]

[Cu(^{iPr}PDI)(CH_3CN)][PF_6] (1). The ligand, ^{iPr}PDI, (2.96 g, 6.14 mmol) and [Cu(I)(CH_3CN)$_4$][PF_6] (2.29 g, 6.15 mmol) was dissolved in THF and stirred overnight at room temperature under N_2 atmosphere. The solvent was removed under reduced pressure to obtain a dark crude solid, which was then re-dissolved in THF and filtered through a Pasteur pipet with a glass wool plug and Celite. The filtered THF solution was layered with diethyl ether to afford dark blue crystals of **(1)**, whose FT-IR, ^{1}H and ^{13}C{^{1}H} NMR data indicated the reported structure in literature.[3,4]

[Cu(^{iPr}PDI)(CO)][PF_6] (2). A THF solution consisting of crystals of **(1)** (250 mg, 0.342 mmol, 10 mL) was reacted with excess CO (35 psi) in a Fischer-Porter tube equipped with a pressure gauge. A rapid color change to dark orange was immediately observed. This mixture was stirred vigorously overnight, and was subsequently frozen in the cold-well and layered with diethyl ether to afford dark orange crystals of **(2)**, although they decomposed rapidly when removed from the CO atmosphere. FT-IR (ATR, cm^{-1}): 2960, 2112, 1633, 1589, 1462, 1437, 1254, 829. ^{13}C{^{1}H} NMR (THF-d_8) δ: 169.46, 166.46, 149.82, 142.71, 141.19, 136.59, 127.51, 124.78, 122.97, 117.66, 27.26, 22.78, 22.75, 17.25. ^{1}H NMR (THF-d_8) δ: 8.50 (s, 3H), 7.27 – 7.15 (m, 6H), 2.87 (m, 4H), 2.45 (s, 6H), 1.17 (dd, 24H, *J* = 9.1, 7.2 Hz).

[Cu(^{iPr}PDI)(Cl)][PF_6] (3). Crystals of **(1)** (0.6253 g, 0.8551 mmol) were dissolved in chloroform and stirred overnight at room temperature. Chloroform was removed under reduced pressure, and the crude solid was re-dissolved in DCM. The filtered DCM solution was layered by pentane to yield dark brown crystals of **(3)** (0.082 g, 0.113 mol, 13%), whose FT-IR spectrum and X-ray structure matched the reported structure in literature.[3] EPR (X-band, THF, 77K): g = 2.05.

[Cu(^{H}PDI)$_2$][PF_6] (4). The ^{H}PDI ligand (0.08 g, 0.3 mmol) and [Cu(I)(CH_3CN)$_4$][PF_6] (0.1 g, 0.3 mmol) were dissolved in acetonitrile and stirred overnight. The mixture was concentrated under reduced pressure. Slow vapor diffusion with diethyl ether yielded purple crystals of **(4)** (0.169 g, 0.120 mol, 40%) and clear crystals of [Cu(I)(CH_3CN)$_4$][PF_6], which were subsequently separated manually. FT-IR (ATR, cm^{-1}): 3081, 2274, 1632, 1591, 1482, 834. ^{1}H NMR (CD_3CN-d_3) δ: 8.14-7.97 (m, 6H), 7.23-7.18 (m, 8H), 7.09-7.04 (m, 4H), 6.50 (d, 8H, *J* = 7.5 Hz), 2.14(s, 12H). ^{13}C{^{1}H} NMR (CD_3CN-d_3) δ: 165.08, 151.92, 149.97, 139.05, 129.81, 127.07, 125.17, 120.38, 17.40. Anal calcd for $C_{42}H_{38}CuN_6P_6F$: C, 60.39; H, 4.59; N, 10.06 Found C, 60.29; H, 4.42; N, 10.47.

X-ray Crystallography. For complexes **1a**, **2** and **3**, single crystal X-ray diffraction data were collected using a Rigaku Oxford Diffraction XtaLABPRO X-ray diffractomter equipped with a Pilatus P200K HPAD detector. Reflections were collected at 100(2) K using graphite-monochromated Mo K_α radiation (λ = 0.71073 Å) using a data collection strategy calculated within CrystalClear to ensure maximum data redundancy and percent completeness.[5] Unit cell determination, initial indexing, data collection, frame integration, Lorentz-polarization corrections and final cell parameter calculations were carried out using CrystalClear. Multi-scan absorption corrections were performed using REQAB.[6] The structures were solved via direct methods using ShelXT and refined using ShelXL in the Olex2 graphical user interface[7] and had their space groups verified by PLATON.[8] The final structural refinement included anisotropic temperature factors on all non-hydrogen atoms. All hydrogen atoms were attached via the riding model at calculated positions using appropriate HFIX commands. The PF_6^- anion in **1a** was found to be disordered over two positions in a 64:36 ratio after the anion, located in the asymmetric unit with elongated fluorine atom ellipsoids, was split into two components related by a free variable and to which were applied suitable crystallographic restraints.

Diffraction intensities for **1** and **4** were collected at 173 K and 223 K, respectively, on a Bruker Apex2 CCD diffractometer using MoKα radiation, λ= 0.71073 Å. Absorption corrections were applied by SADABS.[9] The space group for **4** was determined based on systematic absences. Structures were solved by direct methods and Fourier techniques and refined on F^2 using full matrix least-squares procedures. All non-H atoms were refined with anisotropic thermal parameters. All H atoms were refined in calculated positions in a rigid group model. For both crystals, diffraction at high angles was relatively weak due to flexibility of the terminal groups and a disorder for PF_6^- counter-ions and solvent THF molecules. Thus diffraction data were collected up to $2\vartheta_{max}$ = 56.0°, but only reflections with $2\vartheta_{max}$ = 50.0° have been used in the refinement. The structure of **1** was solved in non-centro symmetrical space group P1 with two independent molecules. The found value of the parameter, 0.057(8), confirms the correct choice of the space group for **1**. The structure of **1** has also two solvent THF molecules. One of these solvent THF molecules is disordered over two positions. Both solvent molecules in **1** were refined with restrictions; the standard C-C and C-O bond distances were used in the refinement as targets for corresponding bonds. The atoms in the disordered THF molecule were refined with isotropic thermal parameters. This THF molecule was modeled as disordered over two positions, but the disorder seems to be more complicated; as in the current model there are two short H…H contacts, around 1.8 Å, between the disordered THF molecule and the cations which are significantly shorter than the standard value of H…H contacts, 2.4 Å. The PF_6^- counter-ion in **4** is also disordered over two positions and was refined with restrictions: the standard P-F bond distance was used in the refinement as a target for corresponding bonds. All calculations were

performed by the Bruker SHELXL-2013 package.[10] The crystallographic data for **1-4** are listed in Table S1.

Computational Methods. Atomic structures were optimized and the character of crystal orbitals computed using density functional theory (DFT) within the Perdew-Burke-Ernzerhof (PBE) functional,[11] using the VASP package[12] and PAW potentials[13] at the Extreme Science and Engineering Discovery Environment (XSEDE).[14] For comparison, the same calculations were performed using van der Waals corrections to PBE within the Tkachenko-Scheffler method (DFT-PBE-TS),[15] which has been shown to capture the experimental geometries of many molecular crystals more closely than DFT-PBE.[16] In the spin constrained systems of **1**, **1a**, and **2** (see Tables S2-S4) the magnetic moments were constrained such that the unit cell had two more spin-up electrons than spin-down electrons per copper atom. The highest occupied crystal orbitals were Cu 3d states, forcing the copper atoms from Cu(I) (d10) to Cu(II) (d9).

Electrochemistry. Cyclic voltammetry was carried out using a Pine WaveNow potentiostat employing a standard three-electrode electrochemical cell consisting of a glassy carbon working electrode, platinum auxiliary electrode and a $Ag/AgNO_3$ reference electrode with a vycor tip filled with acetonitrile. All potentials were internally referenced to the ferrocene redox couple. Unless otherwise noted, experiments were carried out under N_2 at room temperature using solutions of 0.001 M analyte with 0.100 M tetra(n-butyl)ammonium hexafluorophosphate ($TBAPF_6$). All reversibility studies were carried out at 50, 100, 150, 200 and 250 mV/s.

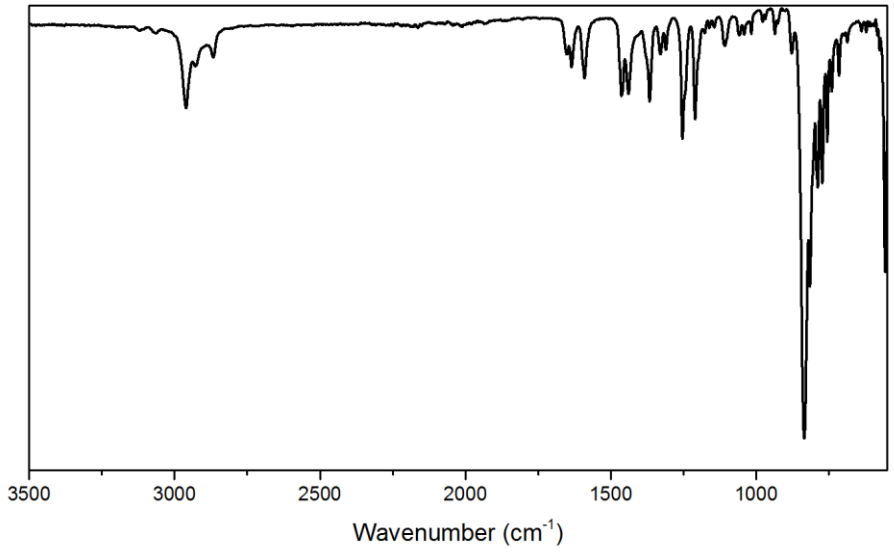

Figure S1. ATR-FT-IR spectrum of [Cu(^{iPr}PDI)(CH_3CN)][PF_6] (**1**).

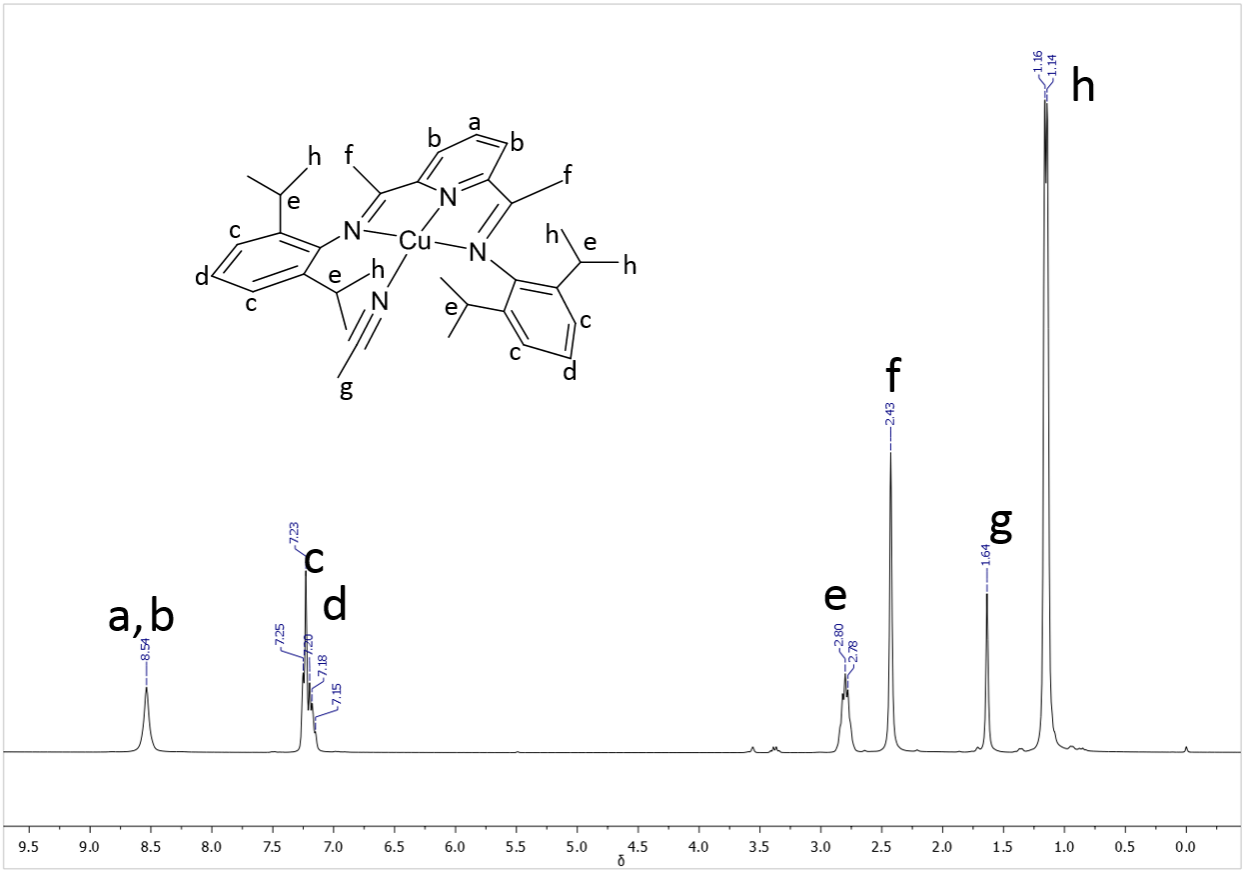

Figure S2. ^{1}H NMR of [Cu(^{iPr}PDI)(CH_3CN)][PF_6] (**1**), THF-d_8. The peaks are likley broadened due to a small amount of Cu(II) inpurity due to slow decomposition in the NMR solvent over time.

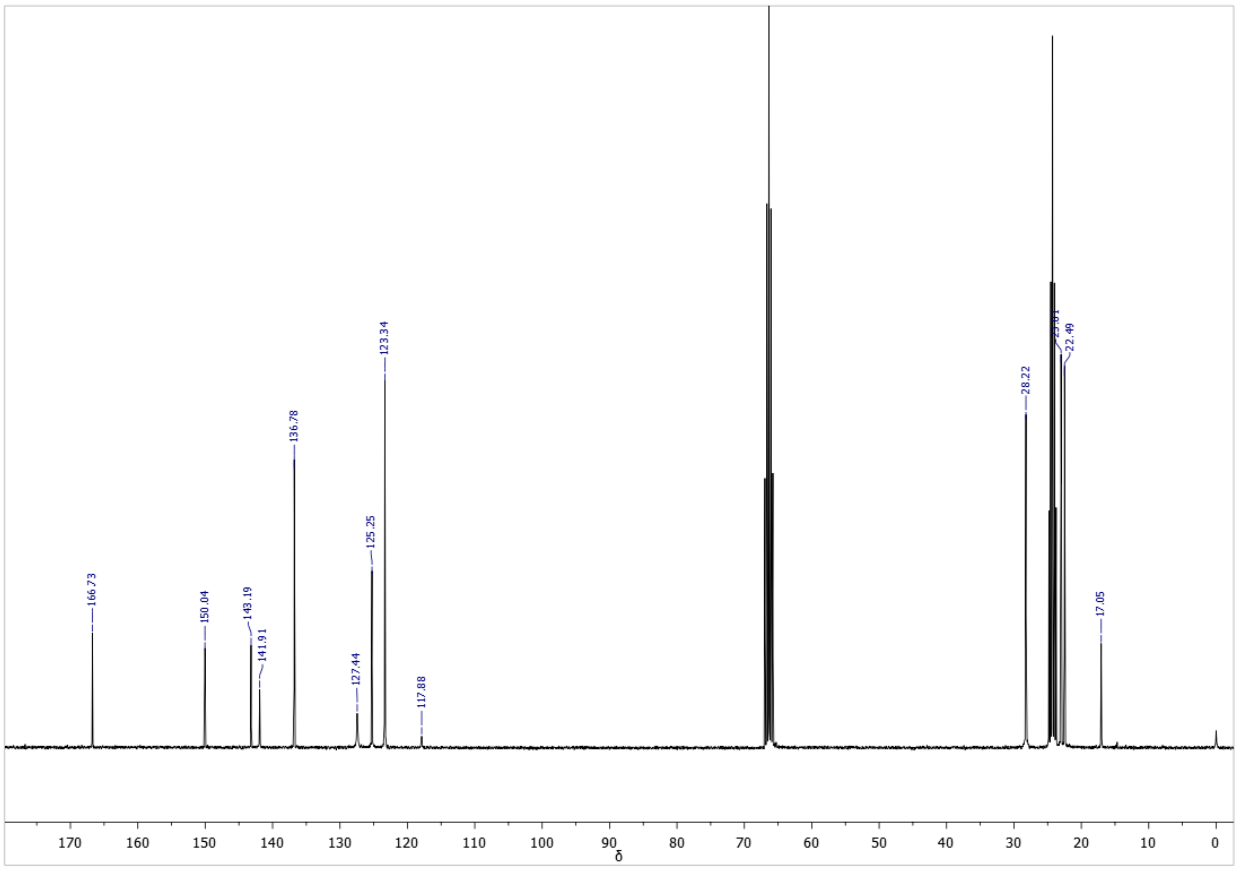

Figure S3. $^{13}C\{^{1}H\}$ NMR of [Cu($^{i\text{Pr}}$PDI)(CH_3CN)][PF_6] (**1**), THF-d_8.

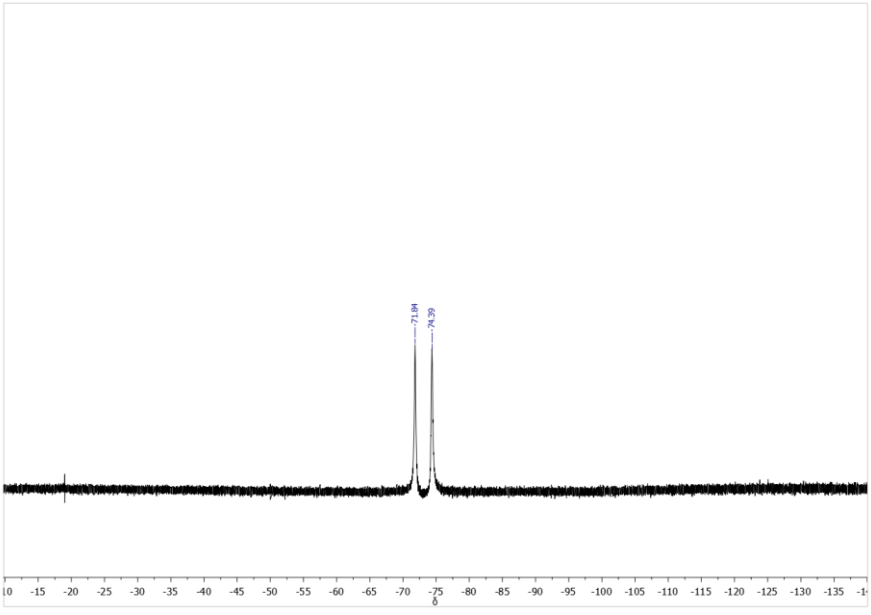

Figure S4. $^{19}F\{^{13}C\}$ NMR of [Cu($^{i\text{Pr}}$PDI)(CH_3CN)][PF_6] (**1**), THF-d_8.

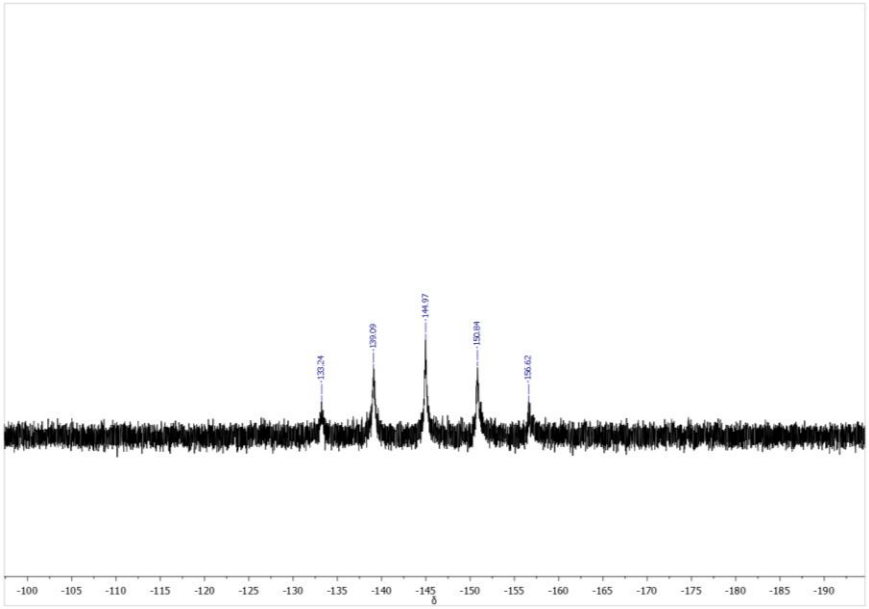

Figure S5. $^{31}P\{^{1}H\}$ NMR of [Cu(^{iPr}PDI)(CH_3CN)][PF_6] (**1**), THF-d_8.

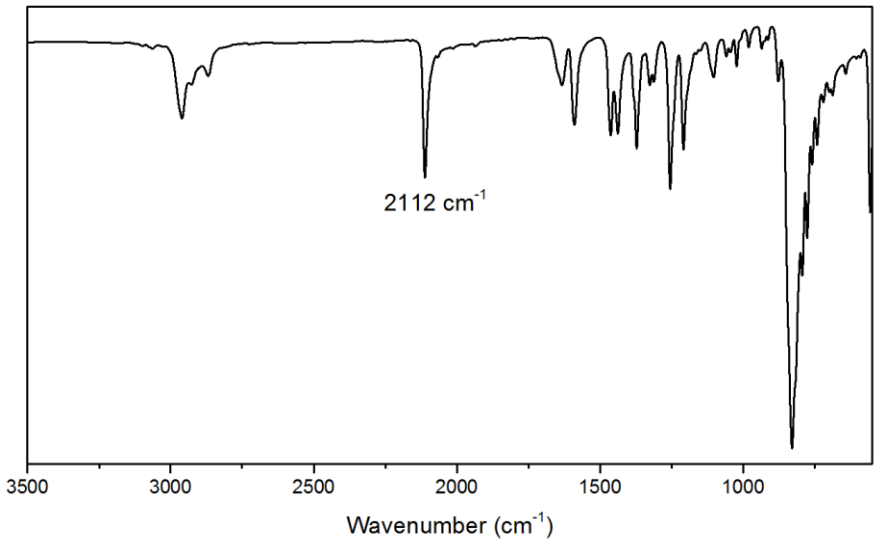

Figure S6. ATR-FT-IR of [Cu($^{i\text{Pr}}$PDI)(CO)][PF_6] (**2**).

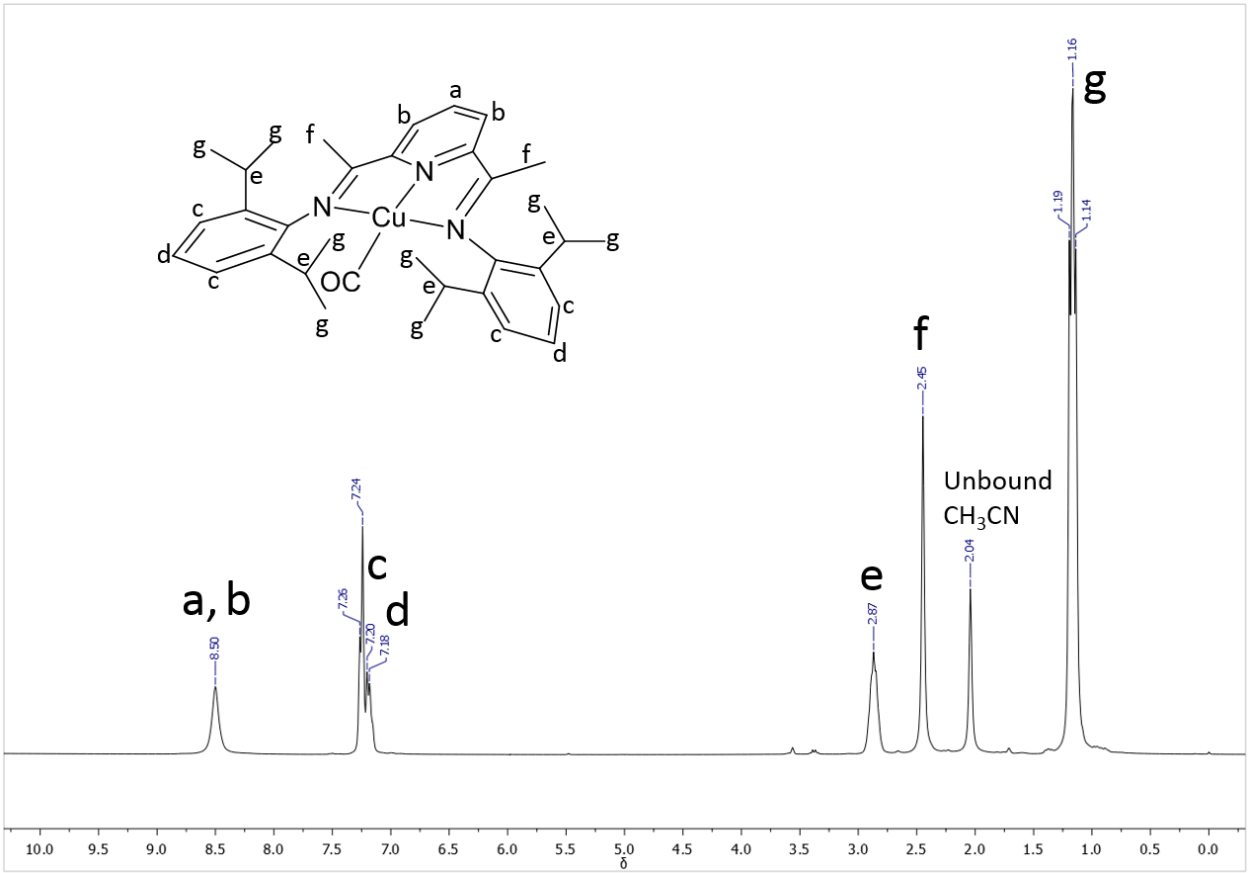

Figure S7. $^{1}H\{^{1}H\}$ NMR of (**2**), THF-d_8. Sample was prepared by sparging CO through a titration NMR tube containing **(1).** The chemical shift at 2.04 ppm indicated the unbound CH_3CN replaced by CO. The peaks are broadened due to a small amount of Cu(II) inpurity due to slow decomposition in the NMR solvent over time.

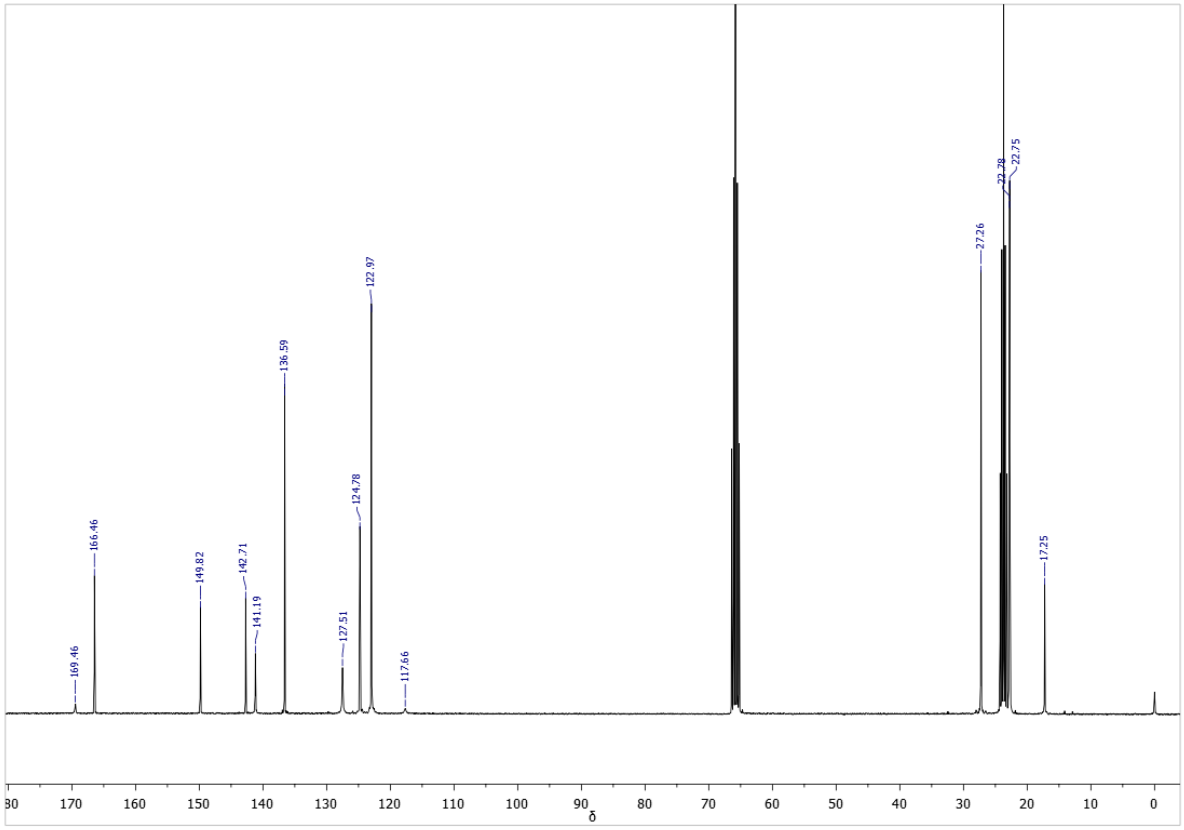

Figure S8. $^{13}C\{^{1}H\}$ NMR of (**2**), THF-d_8. Sample was prepared by sparging CO through an NMR tube containing (**1**)**.** The chemical shift at 117.66 ppm indicated the unbound CH_3CN replaced by CO (169.46 ppm).

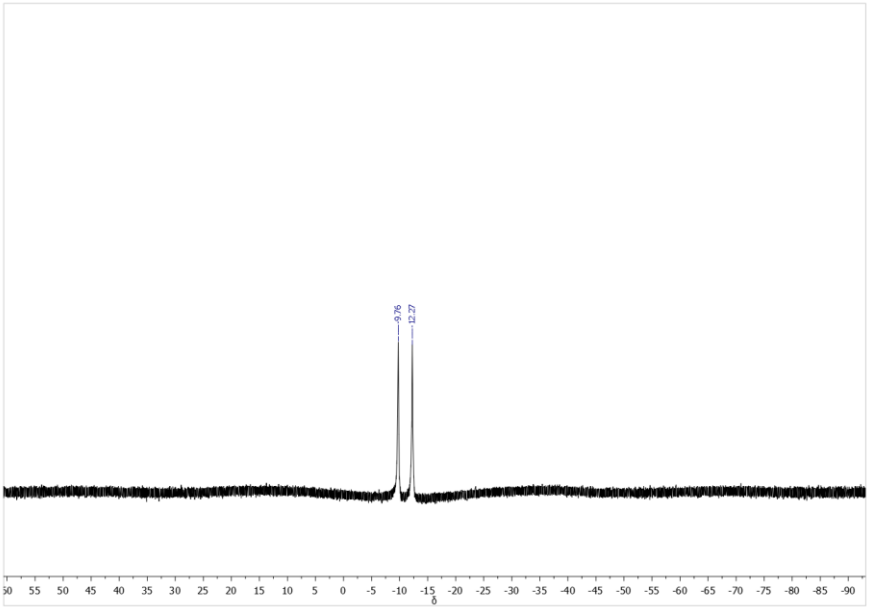

Figure S9. $^{19}F\{^{13}C\}$ NMR of (**2**), THF-d_8.

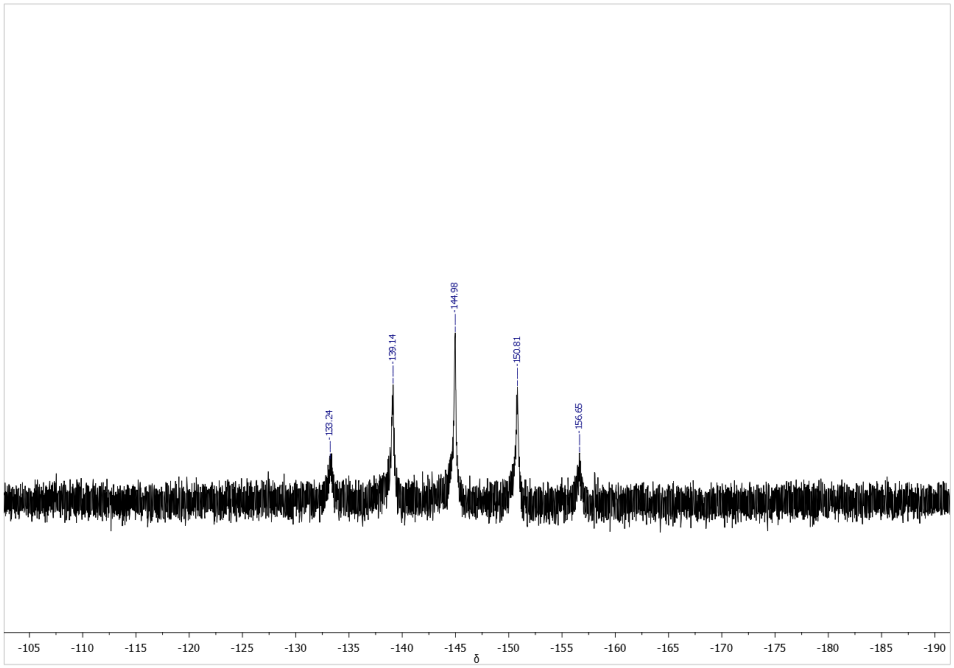

Figure S10. $^{31}P\{^{1}H\}$ NMR of (**2**), THF-d_8.

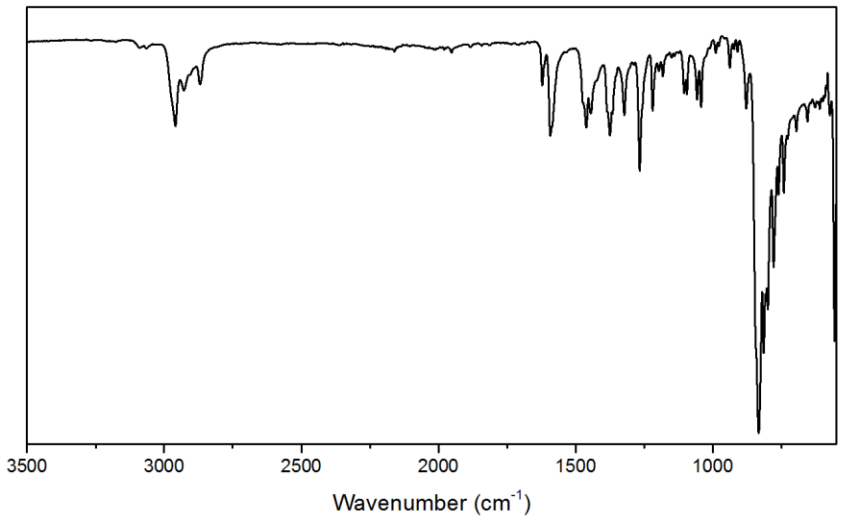

Figure S11. ATR-FTIR of [Cu(^{iPr}PDI)(Cl)][PF_6] (**3**).

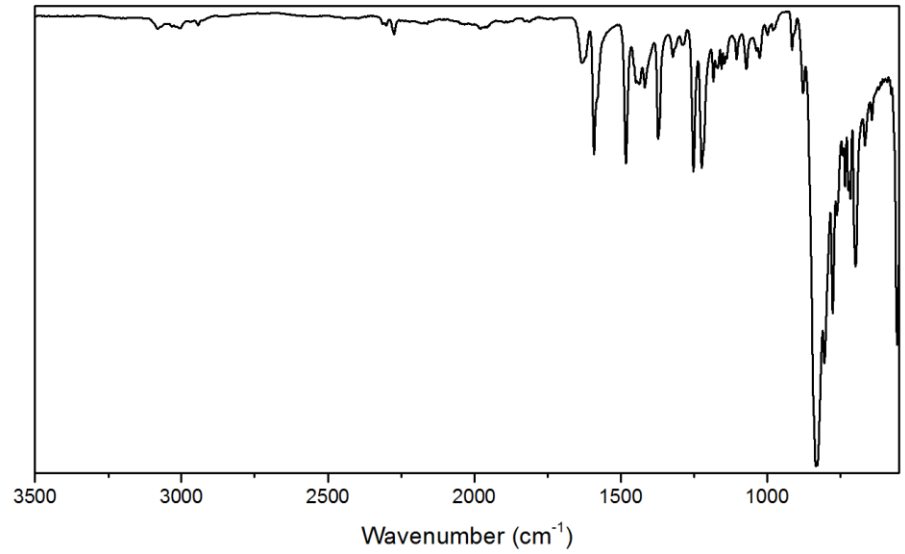

Figure S12. ATR-FT-IR of [Cu(^{H}PDI)$_2$][PF_6] **(4).**

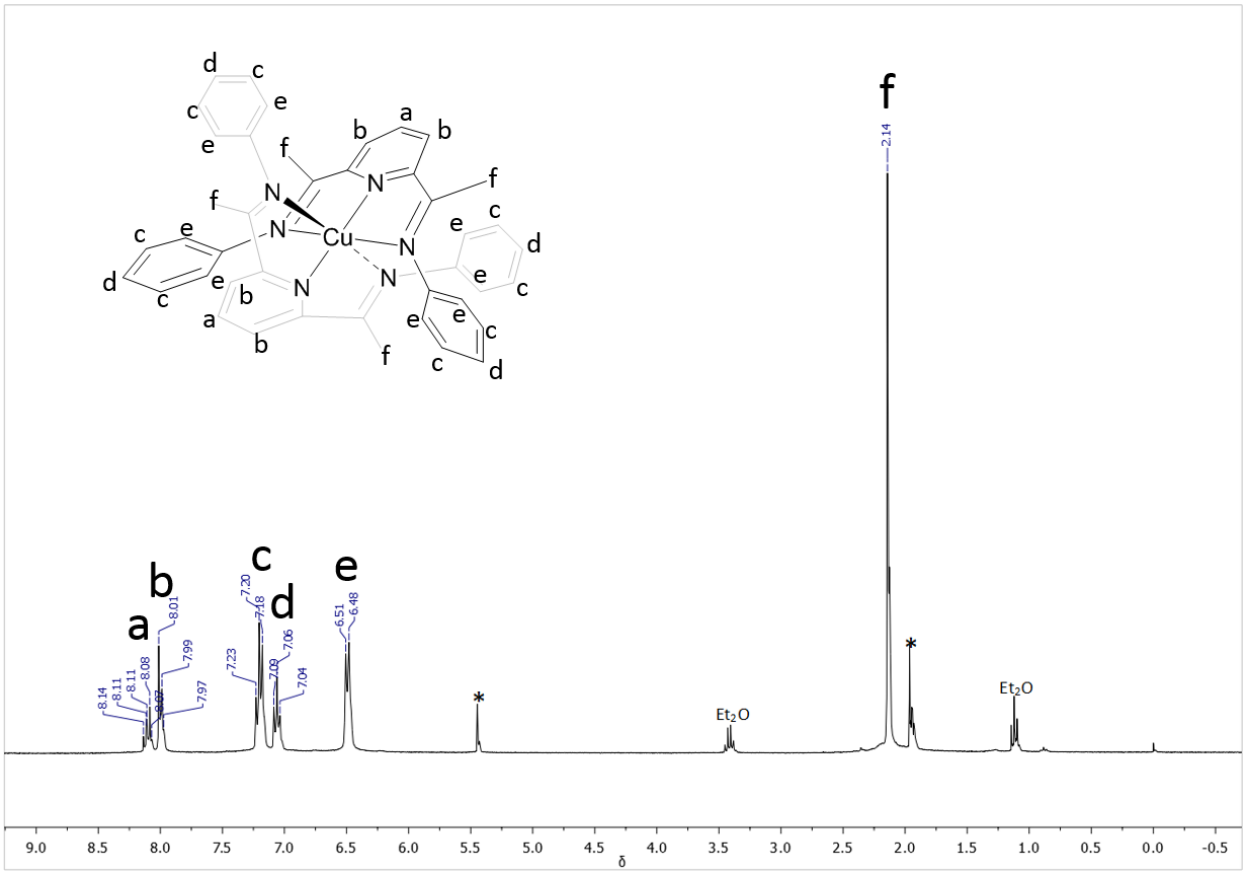

Figure S13. ^{1}H NMR of [Cu(^{H}PDI)$_2$][PF$_6$] (**4**), 300 MHz, CD_3CN (* represents solvent). For clarification, only the cation of **(4)** is shown for peak assignment.

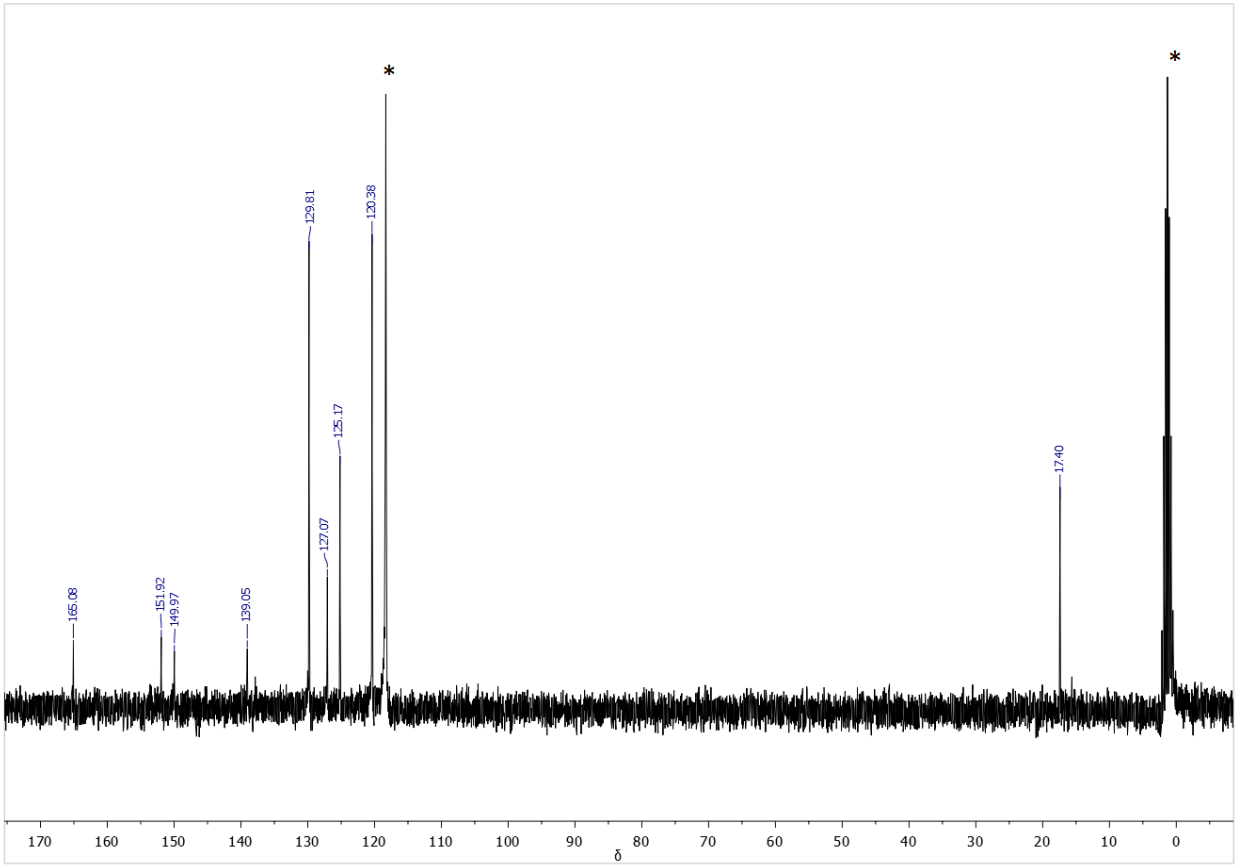

Figure S14. $^{13}C\{^{1}H\}$ NMR of $[Cu(^{H}PDI)_2][PF_6]$ (**4**), CD_3CN (* represents solvent).

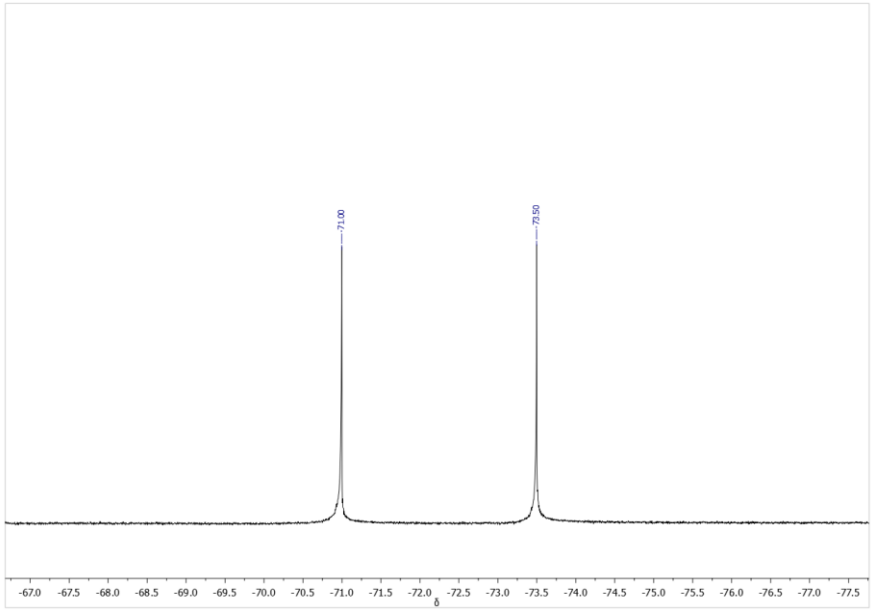

Figure S15. $^{19}F\{^{13}C\}$ NMR of $[Cu(^{H}PDI)_2][PF_6]$ (**4**), CD_3CN.

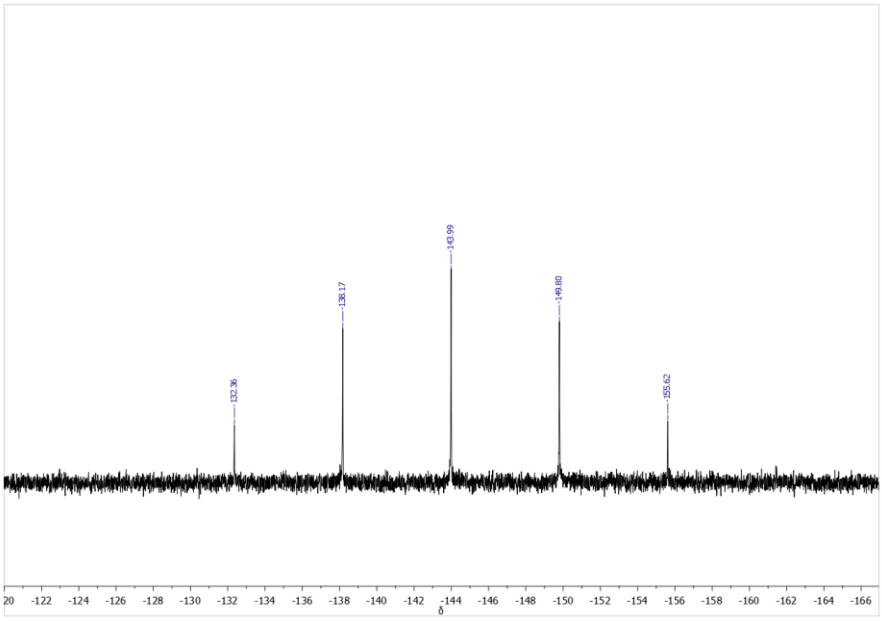

Figure S16. $^{31}P\{^{1}H\}$ NMR of $[Cu(^{H}PDI)_2][PF_6]$ (**4**), CD_3CN.

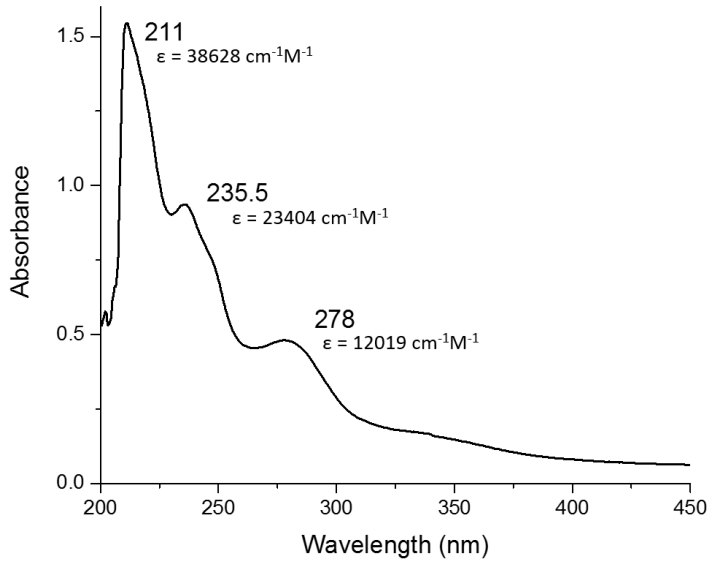

Figure S17. UV-Vis spectrum of 0.04 mM [Cu($^{i\text{Pr}}$PDI)(CH_3CN)][PF_6] (**1**) in THF.

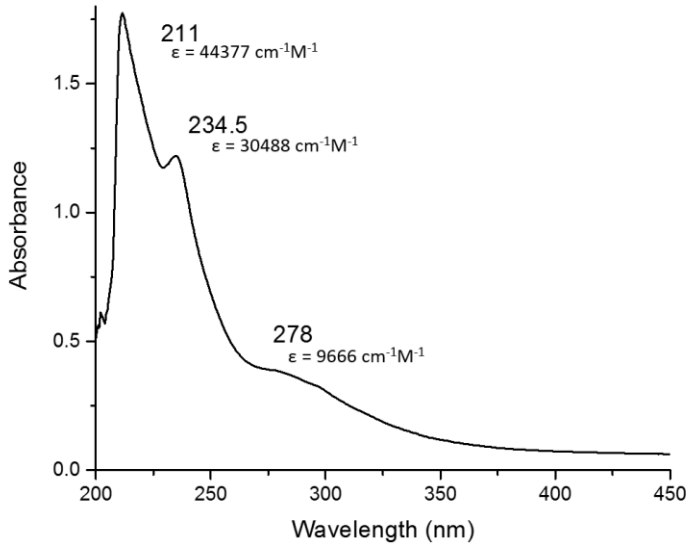

Figure S18. UV-Vis spectrum of [Cu($^{i\text{Pr}}$PDI)(CO)][PF_6] (**2**) under a CO atmosphere in THF.

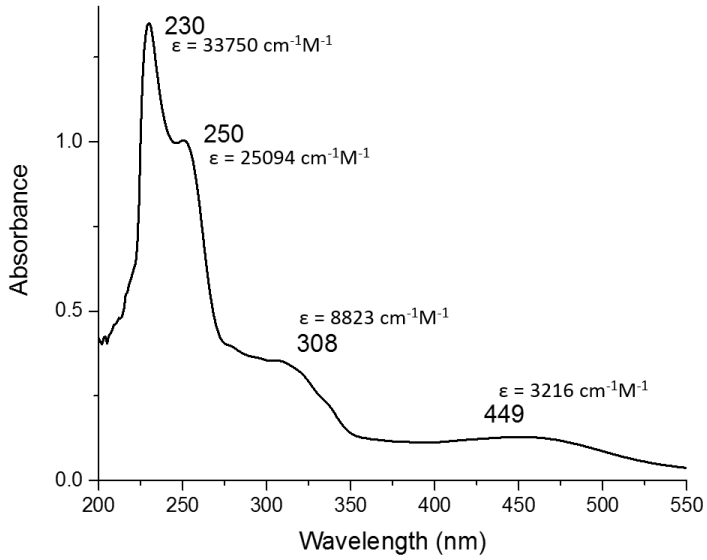

Figure S19. UV-Vis spectrum of 0.04 mM [Cu(^{iPr}PDI)(Cl)PF_6] (**3**) in DCM.

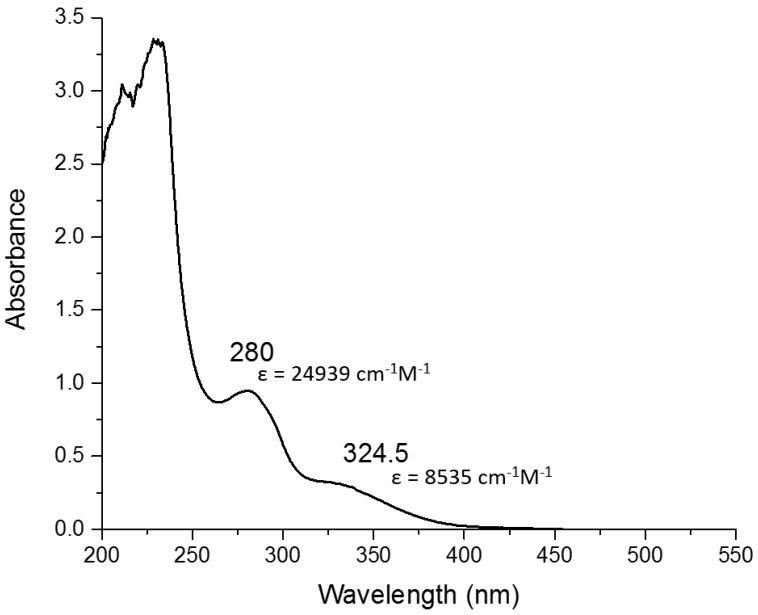

Figure S20. UV-Vis spectrum of 0.038 mM [Cu(^{H}PDI)$_2$][PF_6] (**4**) in CH_3CN.

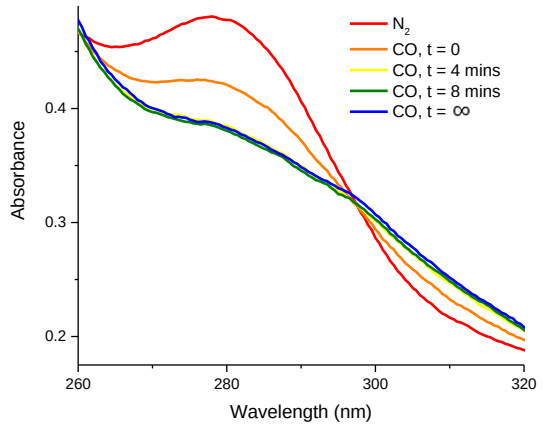

Figure S21. UV-Vis spectrum of the CO reaction with 0.04 mM [Cu($^{i\text{Pr}}$PDI)(CH_3CN)][PF_6] (**1**) in THF. A portion of 1 mL 20 psi CO was added to the headspace in the septum-capped quartz cuvette containing (**1**). (**1**) (red line) gradually changed to [Cu($^{i\text{Pr}}$PDI)(CO)][PF_6] (**2**) (blue line).

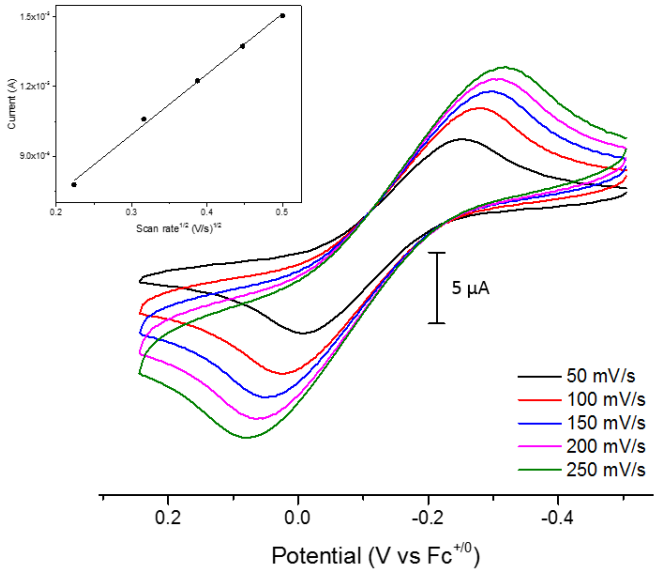

Figure S22. Reversibility study of $Cu^{II/I}$ in 0.001 M [Cu($^{i\text{Pr}}$PDI)(CH_3CN)][PF_6] (**1**) and 0.1 M $TBAPF_6$ in THF. Linear fit of anodic peak currents versus the square root of scan rates is shown (R^2 = 0.996).

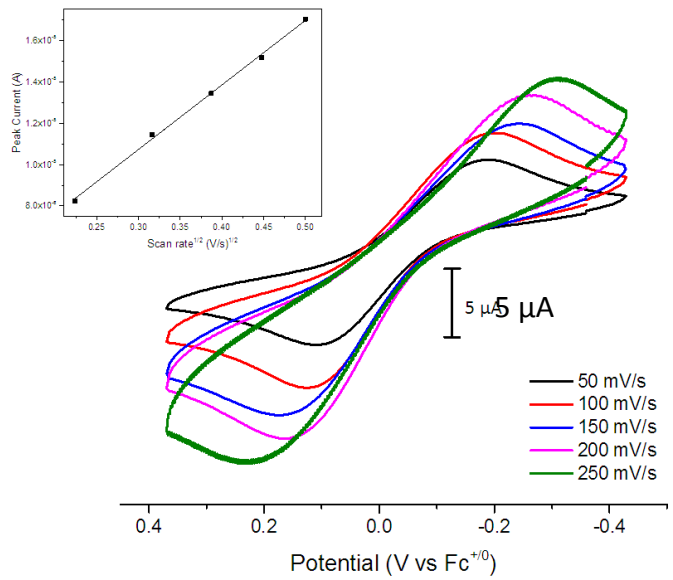

Figure S23. Reversibility study of $Cu^{II/I}$ in 0.001 M [Cu(^{iPr}PDI)(CO)][PF_6] (**2**) and 0.1 M $TBAPF_6$ in THF under a CO atmosphere. Linear fit of anodic peak currents versus the square root of scan rates is shown (R^2 = 0.998).

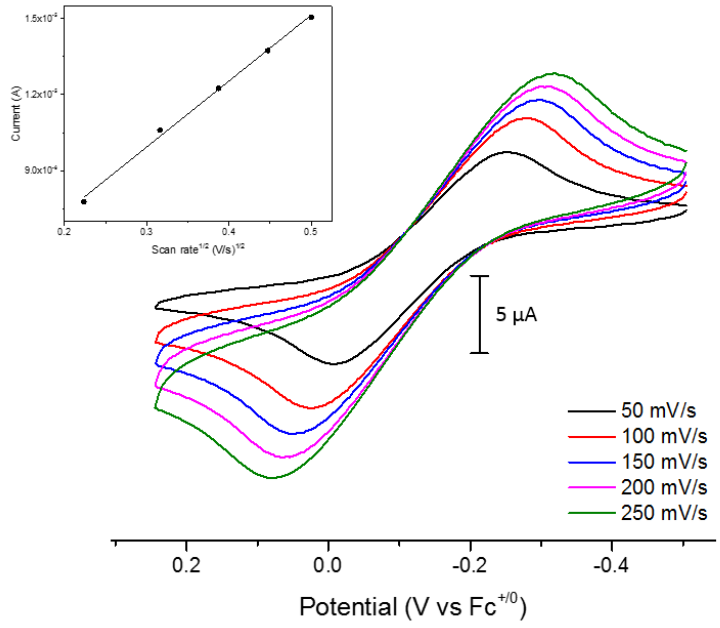

Figure S24. Reversibility study of $Cu^{II/I}$ in 0.001 M [Cu(^{iPr}PDI)(Cl)PF_6] (**3**) and 0.1 M $TBAPF_6$ in DCM. Linear fit of cathodic peak currents versus the square root of scan rates is shown (R^2 = 0.999).

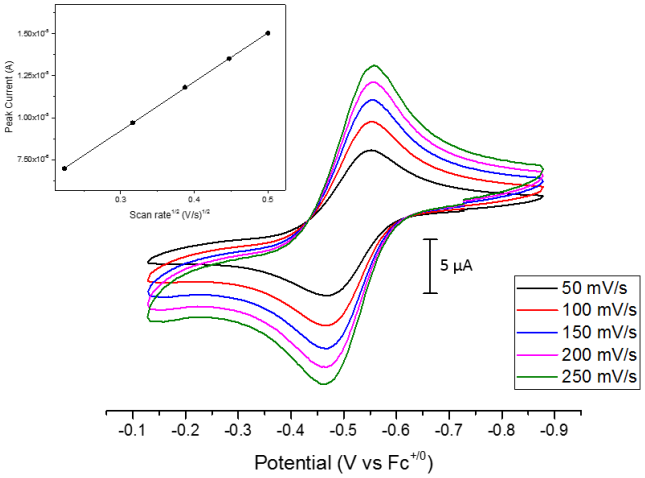

Figure S25. Reversibility study of $Cu^{II/I}$ in 0.001 M $[Cu(^{H}PDI)_2][PF_6]$ (**4**) and 0.1 M $TBAPF_6$ in MeCN. Linear fit of anodic peak currents versus the square root of scan rates is shown (R^2 = 0.999).

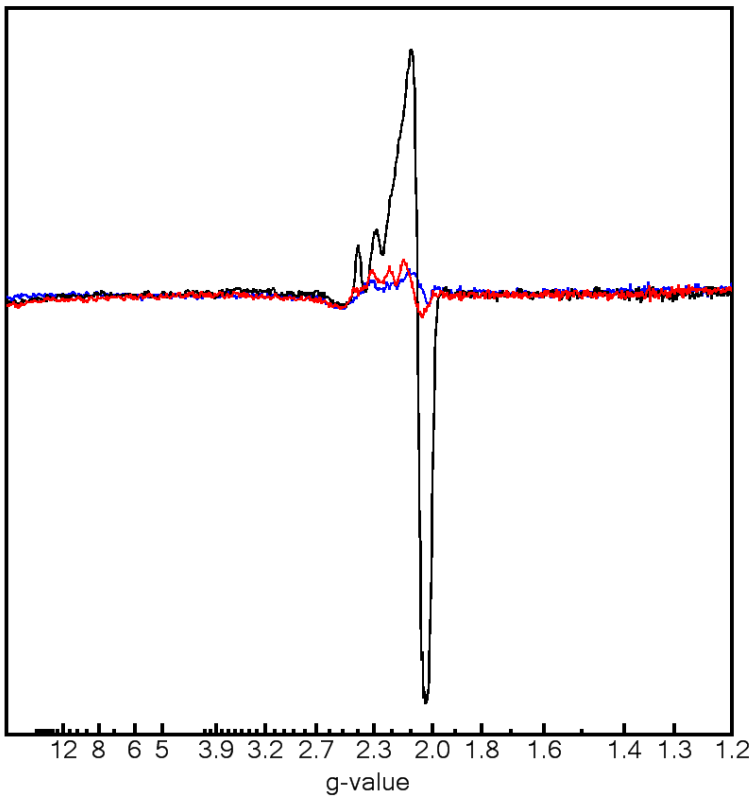

Figure S26. Overlayed EPR spectra of 1mM solutions (THF) of **1** (red), **3** (black), and **4** (blue). (X-band, 77K). Note the small Cu(II) impurity in **1** and **4** (less than 10% by double integration, likely due to slow decomposition in THF).

Table S1. Crystallographic Data for **1**-**4**.

	1	**1a**	**2**	**3**	**4**
Empirical formula	$C_{35}H_{46}CuF_6N_4P \cdot C_4H_8O$	$C_{35}H_{46}CuF_6N_4P$	$C_{34}H_{43}CuF_6N_3OP$	$C_{33}H_{43}ClCuF_6N_3P$	$C_{42}H_{38}CuF_6N_6P$
Formula weight	803.37	731.27	718.22	725.66	835.29
Temperature/K	173(2)	173(2)	173(2)	173(2)	223(2)
Crystal system	triclinic	monoclinic	monoclinic	monoclinic	monoclinic
Space group	P1	$P2_1/c$	$P2_1$	$P2_1$	$P2_1/n$
a/Å	12.4078(19)	8.96(3)	8.8683(7)	8.6259(6)	14.8812(19)
b/Å	13.287(2)	24.20(8)	12.1402(9)	11.8633(8)	17.179(2)
c/Å	14.052(2)	17.53(5)	16.1427(13)	16.6506(12)	15.5446(18)
α/°	96.920(3)	90	90	90	90
β/°	105.670(3)	104.8	100.426(8)	100.785(8)	95.597(2)
γ/°	107.141(3)	90	90	90	90
Volume/$Å^3$	2080.5(6)	3675(20)	1709.3(2)	1673.8(2)	3955.0(8)
Z	2	4	2	2	4
$\rho_{calc}g/cm^3$	1.282	1.322	1.395	1.44	1.403
μ/mm^{-1}	0.624	0.698	0.75	0.841	0.66
F(000)	844	1528	748	754	1720
λ (Å)	0.71073	0.71073	0.71073	0.71073	0.71073
2Θ range °	3.084 to 49.998	4.702 to 52.744	4.224 to 54.998	5.814 to 55.528	3.542 to 56.692
Reflections collected	48577	28473	15278	14835	38883
Ind reflectns (R_{int})	14571 (0.0725)	7478 (0.1766)	7422 (0.0626)	6867 (0.0539)	9748 (0.0645)
GOF	1.017	0.941	0.986	1.025	1.008
R_1, wR_2	0.0525, 0.1311	0.0888, 0.2701	0.0445, 0.1413	0.0657, 0.1860	0.0512, 0.1335
Max/min residual e density (e $Å^{-3}$)	0.37/-0.34	1.78/-1.27	0.50/-0.79	2.30/-1.38	0.78/-0.68

Table S2. Selected Experimental and DFT computed bond lengths (Å) and angles (°) for [Cu(^{iPr}PDI)(CH_3CN)][PF_6] (**1**), both independent molecules in the unit cell.

	1 Experiment	**1** Experiment	**1** DFT-PBE Cu(I)PDI	**1** DFT-PBE-TS Cu(I)PDI	**1** DFT-PBE, spins constrained [Cu(II)PDI^-]
Cu(1)-N(1)	2.397(6)	2.397(6)	2.25	2.26	2.10
Cu(1)-N(2)	2.038(6)	2.037(6)	1.96	1.96	1.88
Cu(1)-N(3)	2.205(6)	2.227(6)	2.21	2.20	2.10
Cu(1)-N(4)	1.907(7)	1.916(7)	1.88	1.88	1.92
N(1)-C(2)	1.274(9)	1.264(10)	1.30	1.30	1.33
N(3)-C(8)	1.278(9)	1.277(9)	1.30	1.30	1.33
C(2)-C(3)	1.511(11)	1.495(11)	1.48	1.48	1.44
C(7)-C(8)	1.511(10)	1.508(11)	1.48	1.48	1.44
C(3)-C(4)	1.404(10)	1.399(11)	1.40	1.40	1.39
C(4)-C(5)	1.370(11)	1.375(12)	1.39	1.39	1.40
C(5)-C(6)	1.375(11)	1.372(12)	1.39	1.39	1.40
C(6)-C(7)	1.399(10)	1.393(11)	1.40	1.40	1.40
N(2)-Cu(1)-N(4)	163.1(3)	163.4(3)	162.8	162.5	171.5
N(1)-Cu(1)-N(3)	149.4(2)	148.9(2)	150.3	150.1	159.3

Table S3. Selected Experimental and DFT computed bond lengths (Å) and angles (°) for [Cu(^{iPr}PDI)(CH_3CN)][PF_6] (**1a**).

	1a Experiment	**1a** DFT-PBE Cu(I)PDI	**1a** DFT-PBE-TS Cu(I)PDI	**1a** DFT-PBE, spins constrained [Cu(II)PDI^-]
Cu(1)-N(3)	2.457(6)	2.33	2.31	2.10
Cu(1)-N(2)	2.047(5)	1.96	1.96	1.88
Cu(1)-N(1)	2.162(7)	2.21	2.20	2.08
Cu(1)-N(4)	1.912(6)	1.87	1.88	1.92
Cu(1)-F(1A)	3.573(9)	3.68	3.66	3.61
Cu(1)-F(1B)	2.912(9)			
N(1)-C(2)	1.273(6)	1.30	1.30	1.33
N(3)-C(8)	1.289(6)	1.29	1.30	1.33
C(2)-C(3)	1.510(7)	1.48	1.48	1.44
C(7)-C(8)	1.507(7)	1.48	1.48	1.44
C(3)-C(4)	1.380(7)	1.40	1.40	1.40
C(4)-C(5)	1.400(8)	1.39	1.39	1.40
C(5)-C(6)	1.397(8)	1.39	1.39	1.40
C(6)-C(7)	1.393(7)	1.40	1.40	1.40
N(2)-Cu(1)-N(4)	160.34(18)	165.4	165.5,	174.0
N(1)-Cu(1)-N(3)	149.18(16)	153.0	153.0	159.2

Table S4. Selected Experimental and DFT computed bond lengths (Å) and angles (°) for [Cu(^{iPr}PDI)(CO)][PF_6] (**2**).

	2 Experiment	**2** DFT-PBE Cu(I)PDI	**2** DFT-PBE-TS Cu(I)PDI	**2** DFT-PBE, spins constrained [Cu(II)PDI$^-$]
Cu(1)-N(1)	2.330(3)	2.53	2.57	2.10
Cu(1)-N(2)	2.000(3)	2.01	2.02	1.88
Cu(1)-N(3)	2.239(4)	2.06	2.04	2.10
Cu(1)-C(10)	1.776(6)	1.79	1.79	1.85
Cu(1)-F(1)	2.741(4)	2.89	2.82	3.02
N(1)-C(2)	1.261(5)	1.29	1.29	1.32
N(3)-C(8)	1.275(6)	1.30	1.29	1.32
C(2)-C(3)	1.492(5)	1.49	1.49	1.44
C(7)-C(8)	1.495(5)	1.49	1.49	1.45
C(3)-C(4)	1.390(5)	1.40	1.39	1.39
C(4)-C(5)	1.375(6)	1.40	1.40	1.40
C(5)-C(6)	1.380(6)	1.39	1.39	1.40
C(6)-C(7)	1.378(6)	1.40	1.40	1.39
N(2)-Cu(1)-C(10)	162.2(2)	151.0	150.6	167.4
N(1)-Cu(1)-N(3)	145.84(13)	145.7	146.0	158.4

Table S5. Selected Experimental and DFT computed bond lengths (Å) and angles (°) for [Cu(^{iPr}PDI)(Cl)PF_6] (**3**).

	3 Experiment	**3** DFT-PBE Cu(II)PDI	**3** DFT-PBE-TS Cu(II)PDI
Cu(1)-N(1)	2.062(5)	2.10	2.10
Cu(1)-N(2)	1.914(5)	1.92	1.92
Cu(1)-N(3)	2.059(5)	2.10	2.10
Cu(1)-Cl(1)	2.1347(16)	2.15	2.15
Cu(1)-F(1)	2.4847(13)	2.70	2.68
N(1)-C(2)	1.284(8)	1.30	1.30
N(3)-C(8)	1.274(8)	1.30	1.30
C(2)-C(3)	1.482(8)	1.48	1.48
C(7)-C(8)	1.470(8)	1.48	1.48
C(3)-C(4)	1.382(8)	1.40	1.40
C(4)-C(5)	1.388(8)	1.40	1.40
C(5)-C(6)	1.380(9)	1.40	1.40
C(6)-C(7)	1.380(8)	1.40	1.40
N(2)-Cu(1)-Cl(1)	176.43(16)	179.2	179.4
N(1)-Cu(1)-N(3)	157.3(2)	158.1	158.0

Table S6. Selected Experimental and DFT-PBE computed bond lengths (Å) and angles (°) for [Cu(^{H}PDI)$_2$][PF$_6$] (**4**). The DFT-PBE computed structure of [Cu(^{H}PDI)$_2$][PF$_6$] (**4**) is also shown. The H-atoms, PDI arms, and acetyl carbons have been omitted for clarity.

	4 Experiment	**4** DFT-PBE Cu(II)PDI	**4** DFT-PBE-TS Cu(II)PDI
Cu(1)-N(1)	2.180(2)	2.06	2.06
Cu(1)-N(2)	2.049(2)	2.03	2.03
Cu(1)-N(3)	2.451(2)	2.64	2.62
Cu(1)-N(4)	2.078(2)	2.02	2.01
Cu(1)-N(5)	2.096(2)	2.06	2.07
Cu(1)-N(6)	2.736(3)	2.83	2.81
N(1)-C(2)	1.276(3)	1.30	1.30
N(3)-C(8)	1.270(3)	1.29	1.29
N(4)-C(23)	1.274(3)	1.30	1.30
N(6)-C(29)	1.269(3)	1.29	1.29
C(2)-C(3)	1.488(4)	1.48	1.47
C(7)-C(8)	1.497(4)	1.49	1.49
C(23)-C(24)	1.492(4)	1.48	1.48
C(28)-C(29)	1.497(4)	1.49	1.49
N(2)-Cu(1)-N(5)	149.31(8)	142.6	142.8
N(1)-Cu(1)-N(3)	147.61(8)	148.2	148.0

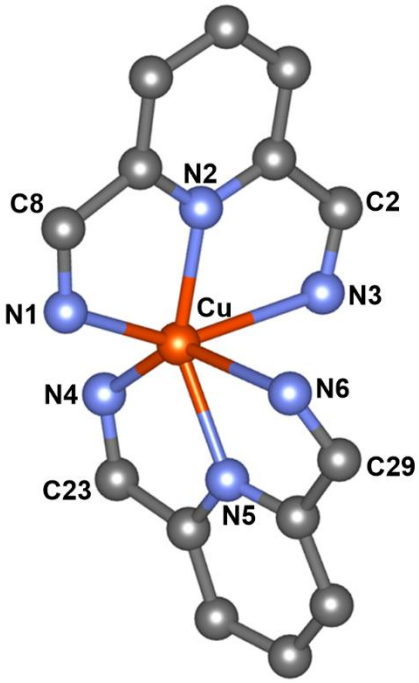

Table S7. Selected Experimental and DFT-PBE computed bond lengths (Å) and angles (°) for [Co(^{iPr}PDI)Cl].[17] The DFT-PBE computed structure is also shown. The H-atoms, PDI arms, and acetyl carbons have been omitted for clarity.

	[Co(^{iPr}PDI)Cl] Experiment (ref 17)	**[Co(^{iPr}PDI)Cl]** DFT-PBE [Co(II)PDI^{-}]	**[Co(^{iPr}PDI)Cl]** DFT-PBE-TS [Co(II)PDI^{-}]
Co(1)-N(1)	1.92	1.89	1.89
Co(1)-N(2)	1.80	1.79	1.79
Co(1)-N(3)	1.91	1.90	1.90
Co(1)-Cl(1)	2.18	2.17	2.17
N(1)-C(2)	1.32	1.33	1.33
N(3)-C(8)	1.32	1.33	1.33
C(2)-C(3)	1.44	1.44	1.44
C(7)-C(8)	1.44	1.44	1.44
N(2)-Co(1)-Cl(1)	179.1	179.7	179.8
N(1)-Co(1)-N(3)	162.9	163.9	164.0

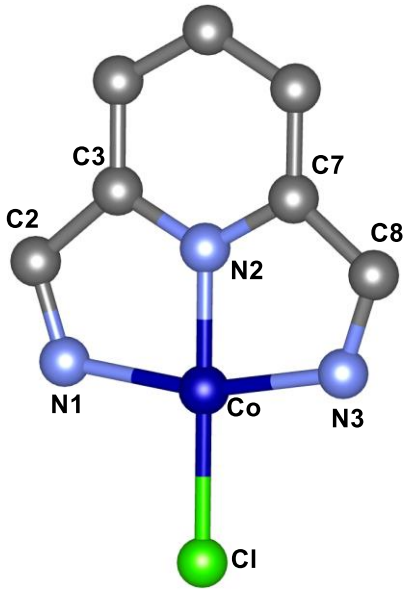

Table S8. Selected Experimental bond lengths (Å) and angles (°) for [Cu($^{i\text{Pr}}$PDI)(CH_3CN)][PF_6] (**1**), (both independent molecules in the unit cell), (**1a**), [Cu($^{i\text{Pr}}$PDI)(CO)][PF_6] (**2**), and [Cu($^{i\text{Pr}}$PDI)(Cl)PF_6] (**3**).

	1	**1**	**1a**	**2**	**3**
Cu(1)-N(1)	2.397(6)	2.397(6)	2.457(6)	2.330(3)	2.062(5)
Cu(1)-N(2)	2.038(6)	2.037(6)	2.047(5)	2.000(3)	1.914(5)
Cu(1)-N(3)	2.205(6)	2.227(6)	2.162(7)	2.239(4)	2.059(5)
Cu(1)-N(4)	1.907(7)	1.916(7)	1.912(6)		
Cu(1)-C(10)				1.776(6)	
Cu(1)-Cl(1)					2.1347(16)
Cu(1)-F(1)			2.913(10)	2.74264(17)	2.4847(13)
Cu(1)-F(1B)			3.572(10)		
N(1)-C(2)	1.274(9)	1.264(10)	1.273(6)	1.261(5)	1.284(8)
N(3)-C(8)	1.278(9)	1.277(9)	1.289(6)	1.275(6)	1.274(8)
C(2)-C(3)	1.511(11)	1.495(11)	1.510(7)	1.492(5)	1.482(8)
C(7)-C(8)	1.511(10)	1.508(11)	1.507(7)	1.495(5)	1.470(8)
N(2)-Cu(1)-N(4)	163.1(3)	163.4(3)	160.34(18)		
N(1)-Cu(1)-N(3)	149.4(2)	148.9(2)	149.18(16)	145.84(13)	157.3(2)
N(2)-Cu(1)-C(10)				162.2(2)	
N(2)-Cu(1)-Cl(1)					176.43(16)

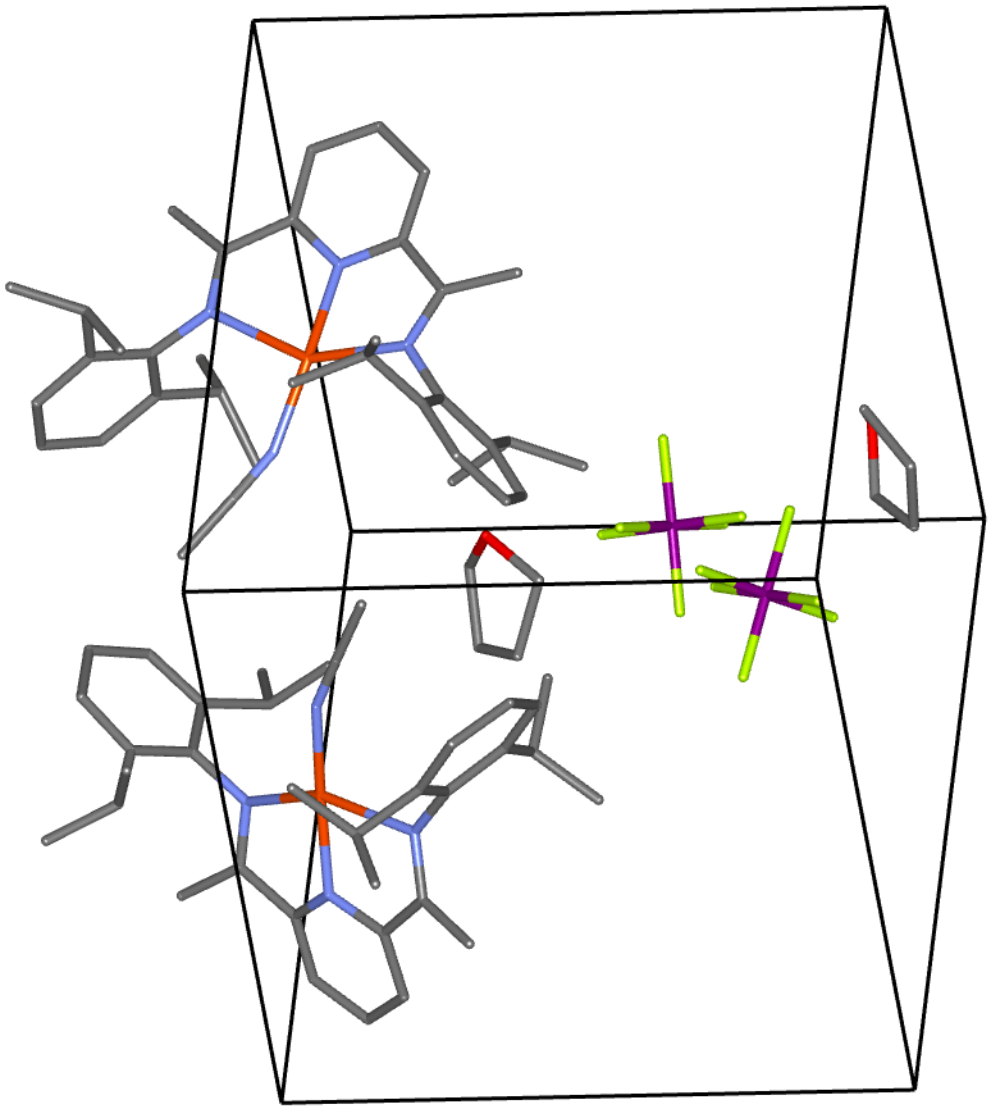

Figure S27. DFT-PBE-TS computed unit cell for [Cu($^{i\text{Pr}}$PDI)(CH_3CN)][PF_6] (**1**).

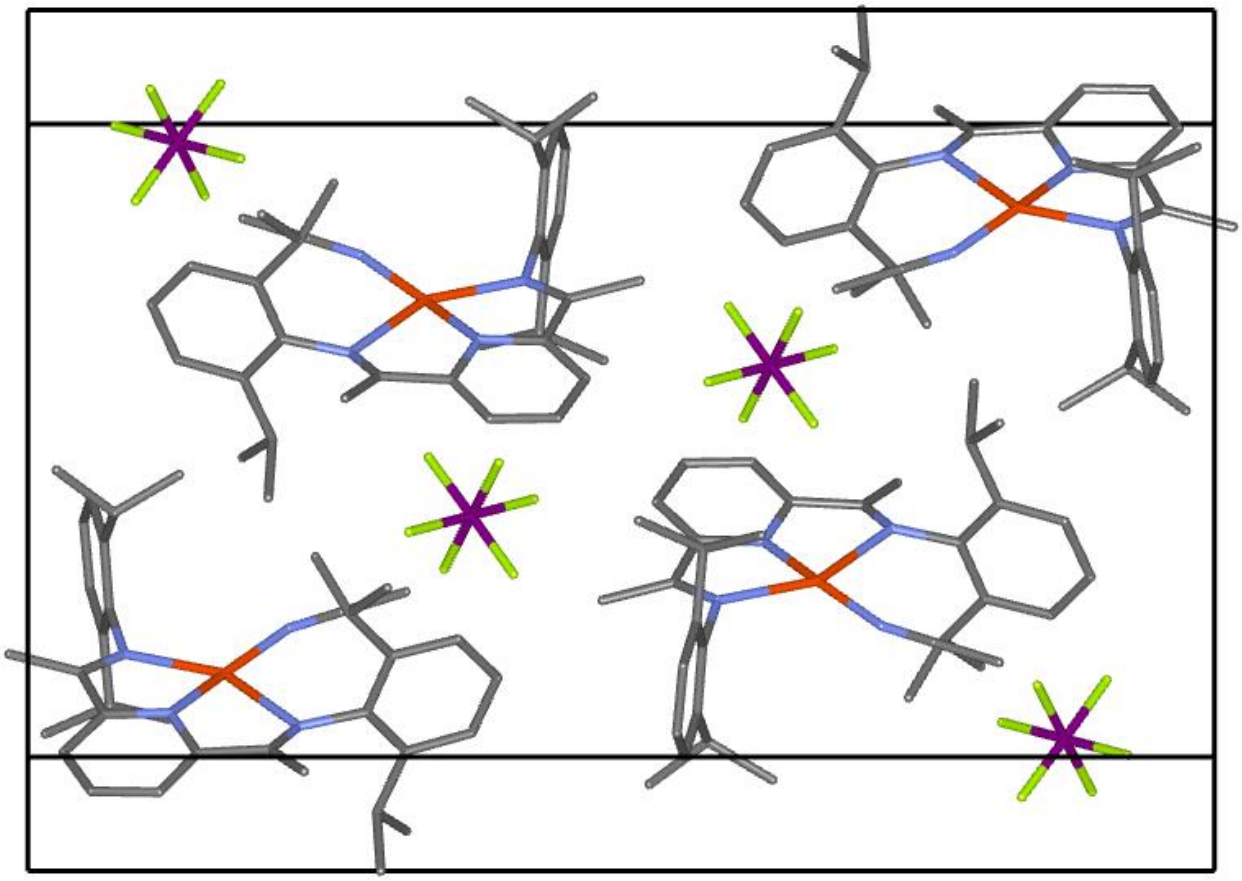

Figure S28. DFT-PBE-TS computed unit cell for [Cu($^{i\text{Pr}}$PDI)(CH_3CN)][PF_6] (**1a**).

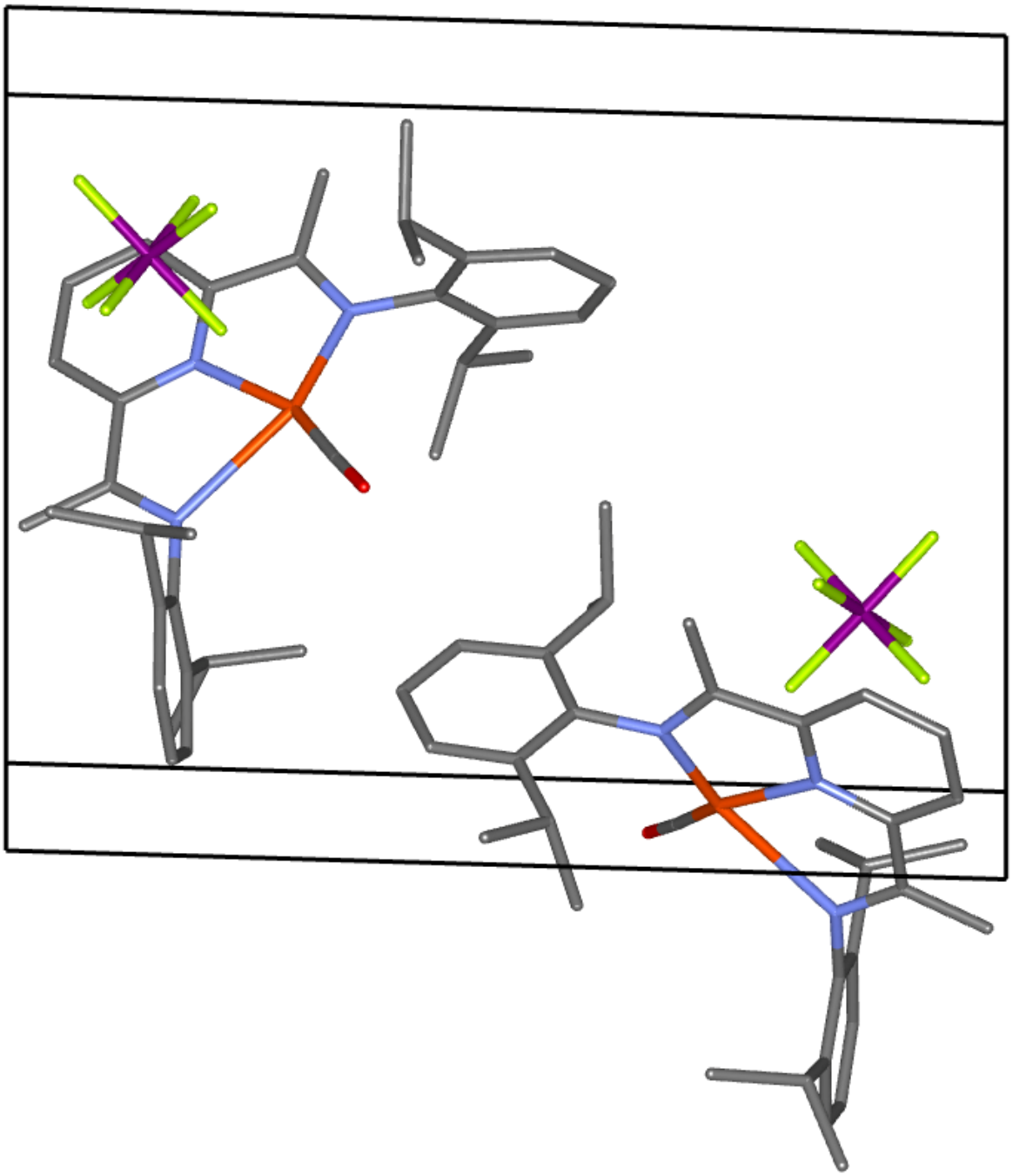

Figure S29. DFT-PBE-TS computed unit cell for [Cu(^{iPr}PDI)(CO)][PF_6] (**2**).

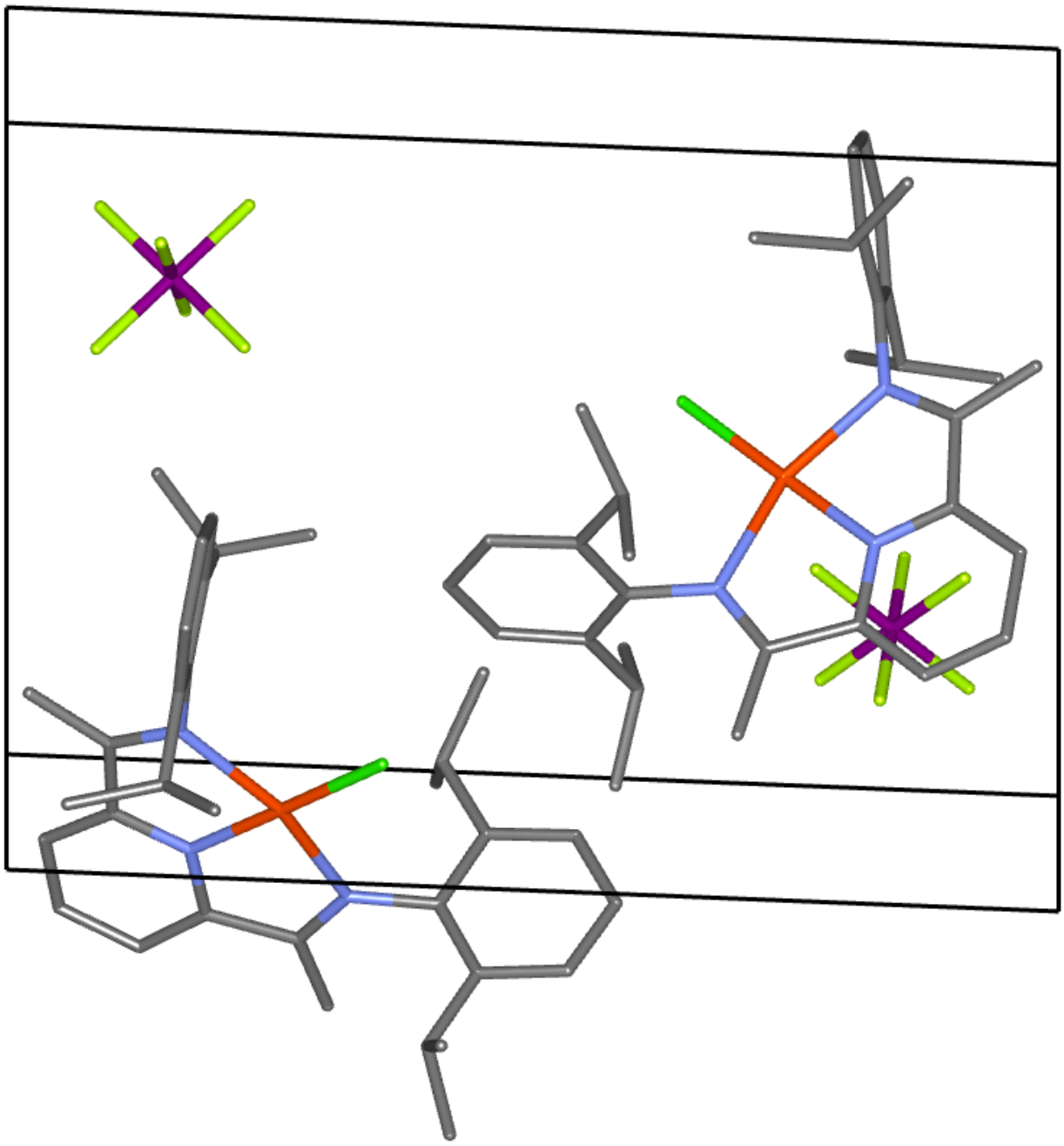

Figure S30. DFT-PBE-TS computed unit cell for [Cu(^{iPr}PDI)(Cl)PF_6] (**3**).

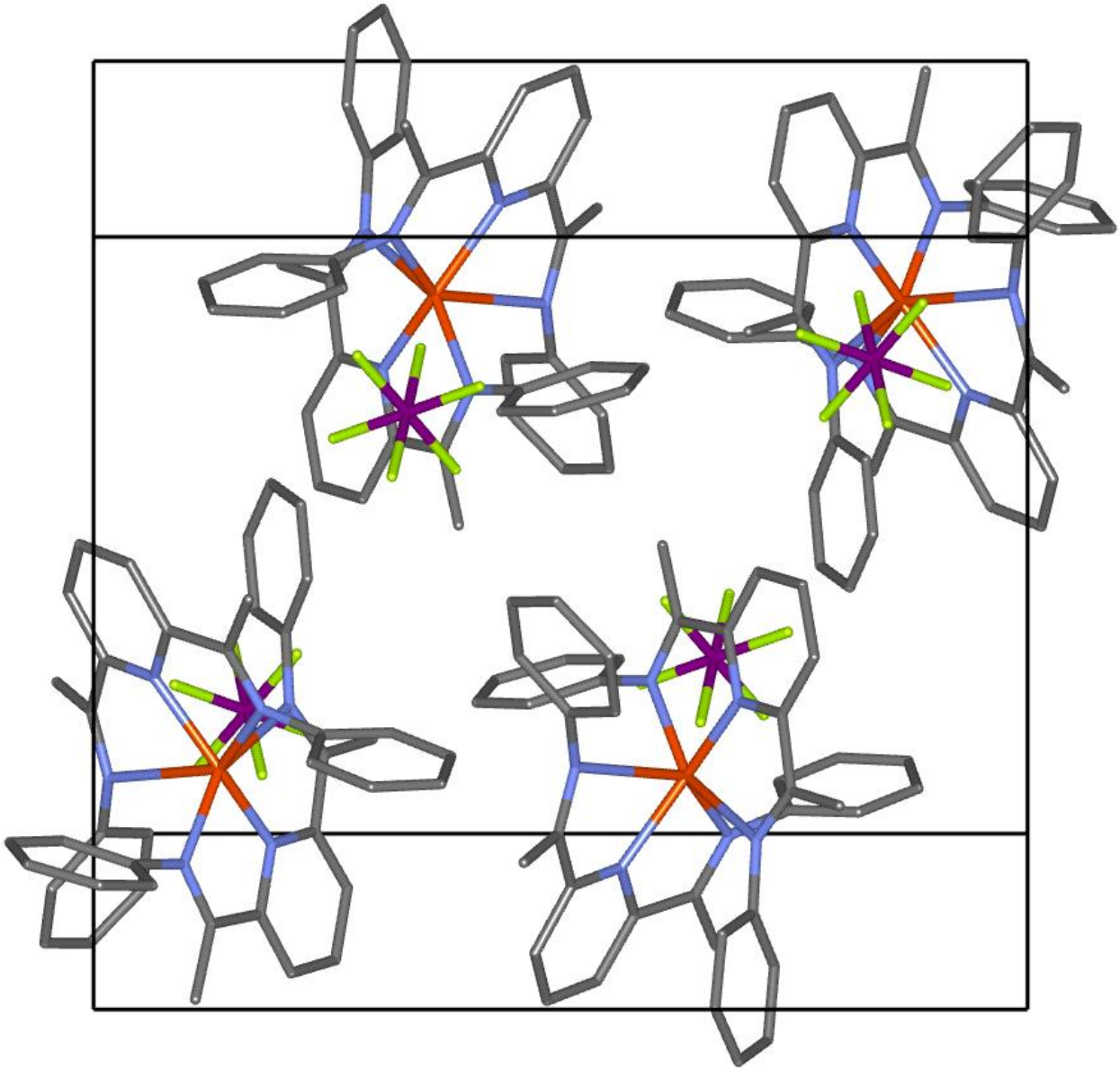

Figure S31. DFT-PBE-TS computed unit cell for $[Cu(^{H}PDI)_2][PF_6]$ (**4**).

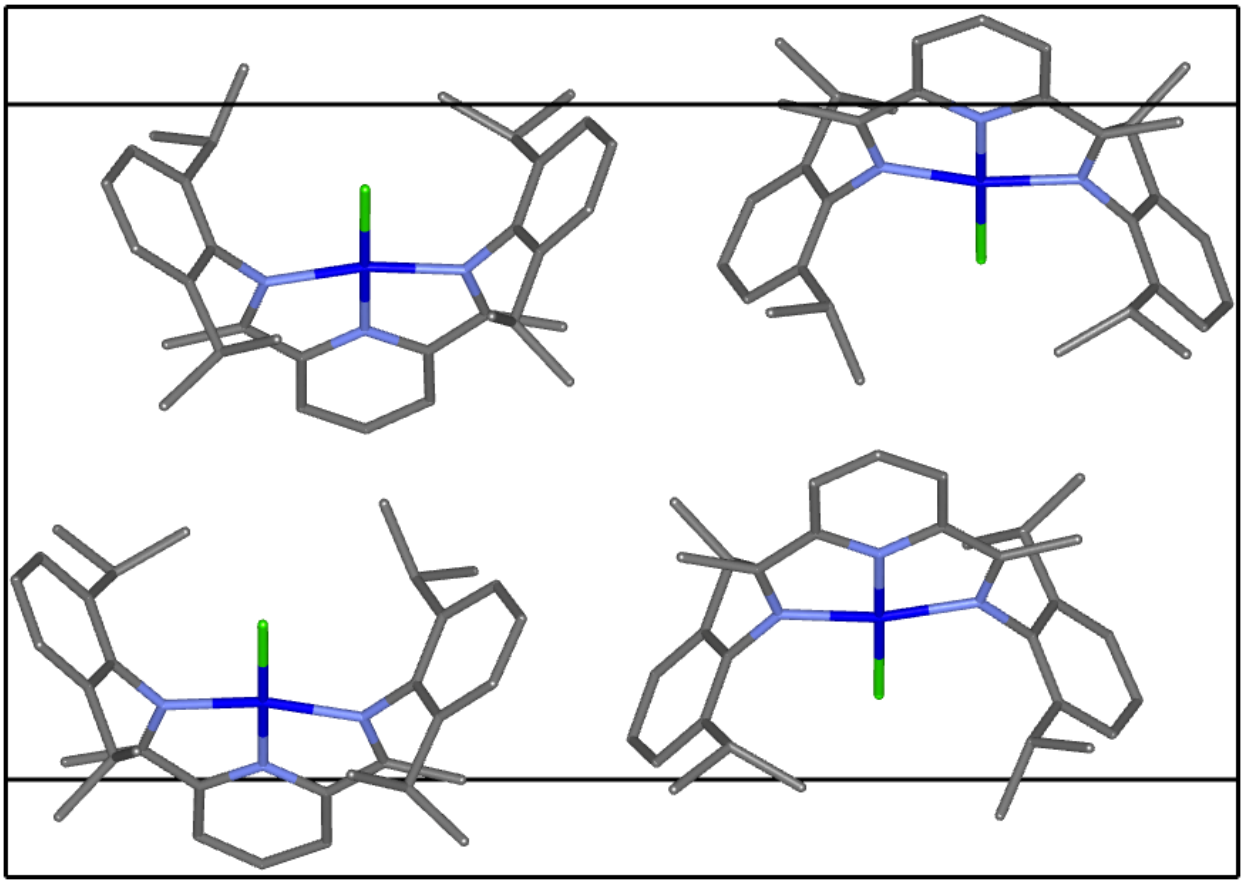

Figure S32. DFT-PBE-TS computed unit cell for [Co(*i*Prr PDI)Cl].[17]

References:

[1] Brooke, L. S.; Brookhart, M.; Bennett A. M. A. *J. Am. Chem. Soc.* 1998, **120**, 4049-4050.
[2] Alyea, E. C.; Merrell, P. H. *Synth. React. Inorg. Met. Org. Chem.* 1974, **4**, 535-544.
[3] Le Gall, B.; Conan, F.; Cosquer, N.; Kerbaol, J. M.; Kubicki, M. M.; Vigier, E.; Le Mest, Y.; Sala Pala, J. *Inorg. Chim. Acta.* 2001, **324**, 300-308.
[4] Le Gall, B.; Conan, F.; Kerbaol, J. M.; Kubicki, M. M.; Vigier, E.; Le Mest, Y.; Sala Pala, J. *Inorg. Chim. Acta.* 2002, **336**, 87-90.
[5] Pflugrath, J.W. *Acta Cryst.* 1999, **D55**, 1718-1725.
[6] Rigaku (1998). REQAB. Rigaku Corporation, Tokyo, Japan.
[7] (a) Sheldrick, G.M. *Acta Cryst.* 2015, **A71**, 3-8. (b) Sheldrick, G.M. *Acta Cryst.* 2008, **A64**, 112-122. (c) Dolomanov, O.V.; Bourhis, L.J.; Gildea, R.J; Howard, J.A.K; Puschmann, H. *J. Appl. Cryst.* 2009, **42**, 339-341.
[8] Spek, A.L. *Acta Cryst.* 2009, **D65**, 148-155.
[9] G. M. Sheldrick, *Bruker/Siemens Area Detector Absorption Correction Program*, Bruker AXS, Madison, WI, 1998.
[10] Sheldrick, G. M. (2008). *Acta Cryst.* **A64**, 112-122.
[11] J.P. Perdew, K. Burke and M. Ernzerhof, *Phys. Rev. Lett.*, 1996, **77**, 3865.
[12] G. Kresse and J. Furthmuller, *Phys. Rev. B,* 1996, **54**, 11169.
[13] G. Kresse and D. Joubert, *Phys. Rev. B*, 1999, **59**, 1758.
[14] John Towns, Timothy Cockerill, Maytal Dahan, Ian Foster, Kelly Gaither, Andrew Grimshaw, Victor Hazlewood, Scott Lathrop, Dave Lifka, Gregory D. Peterson, Ralph Roskies, J. Ray Scott, Nancy Wilkins-Diehr, "XSEDE: Accelerating Scientific Discovery", Computing in Science & Engineering, vol.16, no. 5, pp. 62-74, Sept.-Oct. 2014, doi:10.1109/MCSE.2014.80
[15] A. Tkachenko and M. Scheffler, *Phys. Rev. Lett.*, 2009, **102**, 073005.
[16] T. Bucko, S. Lebegue, J. Hafner and J.G. Angyan, *Phys. Rev. B*, 2013, **87**, 064110.
[17] V. C. Gibson *,* M. Humphries *,* K. Tellmann *,* D. Wass *,* A. J. P. White *,* D. J. Williams*, Chem. Commun.* 2001*,* 2252*.*